

Crystallization temperatures and petrogenetic source of the Neoproterozoic Nagar Parkar granites: deduced from zircon crystal shapes

Marimo NAKABAYASHI¹⁾, Hafiz Ur REHMAN²⁾ *

¹⁾ *Department of Earth and Environmental Sciences, Kagoshima University, Japan*

²⁾ *Graduate School of Science and Engineering, Kagoshima University, Japan*

* Corresponding author's e-mail address: hafiz@sci.kagoshima-u.ac.jp

Abstract: Granitic rocks are widely distributed on earth that are formed by the solidification/crystallization of magma. Most granites contain zircons, an accessory mineral, that preserve records of the magmatic crystallization. In this study, zircons from the Neoproterozoic (750 Ma) Nagar Parkar Igneous Complex were studied for crystal morphology to constrain the temperatures of crystallization. In total, 255 zircon crystals from two granitic varieties (gray and pink granites) were investigated. Majority of the crystals exhibit well-developed {100} and {110} prisms and short {101}, {211} and {121} pyramidal faces. Temperatures estimated from the zircon typology from gray granites ranged from 633–831 °C (n: 24) for sample NGP62a, 650–850 °C (n: 78) for sample NGP62b, 600–850 °C (n: 37) for sample NP01, 675–800 °C (n: 31) for sample NP12, and 613–850 °C (n:56) for sample NP62, and one pink granite sample showed a range from 675–800 °C (n: 7). Average temperatures from the above samples, when compared with the Titanium-in-zircon thermometry and the results were better than or within ± 50 °C for four samples, and within ± 100 °C for other two samples. The data from zircon typology show granodiorites to monzogranites fields, and a few crystals point towards alkaline granites. The zircon morphology suggest that the magma was possibly derived from a crustal origin with minor hybridization of the mantle component.

Keywords: Zircon crystal shapes, thermometry, Ti-in-Zircon, granites, Nagar Parkar Igneous Complex

1. Introduction

Granites are plutonic rocks that are formed from a silica-rich magma that cools slowly and crystallize at a certain depth from the earth's surface. They are widely distributed within the continents as ancient cratons, batholiths or stocks, and form the cores of uplifted islands within the oceans. Granites are dominantly composed of Potash feldspar, plagioclase, quartz with some amphibole, biotite, and accessory ilmenite, apatite, and zircon. Among the other main constituent minerals, zircon (hard and resistant to chemical alteration) is one of the most widely used minerals for geochronology, crustal growth and thermal history of the earth (e.g., [1-4]). It preserves information of the magma source and its external crystal morphology (combination of the crystal {100}, {110}, or {010} prismatic and {101}, {121}, or {211} pyramidal faces) is used to identify its petrogenetic source or provenance, and temperatures of crystallization [3-10]. The most common crystal forms of zircon (Fig. 1), exhibited by high and constant growth rates of {010} with symmetric growth of {110} prisms, are interpreted for alkaline magmas

that were likely emplaced at shallow crustal depths. Whereas, the relative decreasing growth rates of {010} with highly variable and asymmetric growth rates of {011} prisms and {121} pyramids indicate calcalkaline and Al-rich anatectic magmas [3-6].

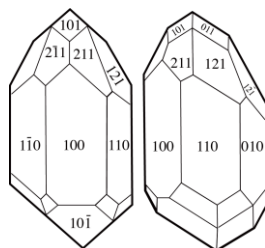


Fig. 1. Typical crystal shape of types {100} and {110} zircon (modified after [11]).

We investigated external and internal morphology of zircon crystals from the Neoproterozoic granites of the Nagar Parkar Igneous Complex (NPIC) (Fig. 2). Two types of granitic plutons (namely the gray and pink granites) are exposed in the NPIC [12-14]. Field and petrographic details of the granites have been reported in past publications, however, the petrogenetic characteristics of magma are not reported yet. To decipher the crystallization temperature of magma and its petrogenetic source, we inspected zircon crystal external shapes following the typological approach of Pupin [5], and internal structures via cathodoluminescence (CL) images following the published literature (e.g., [3, 7, 15-16]). Internal structures of zircons provide strong tool to trace the changes in zircon crystals during their growth. In addition, the relative variation in zircon crystal shape, combined with internal structures, provide useful information for temperatures of the magmatic crystallization and determining their petrogenetic source. Temperature data obtained from the crystal typology were also compared with the Ti-in-zircon thermometry [17] for better understanding.

2. Geological background of the studied samples

The Neoproterozoic granites of the NPIC are situated to the west of the Trans-Aravalli Malani Igneous Suite (MIS) of the Rajasthan or Aravalli Craton of the Indian Shield [18-19 and references therein] (Fig. 2a). Dominant lithological units are the riebeckite-aegirine gray granites and the biotite-hornblende pink granites that are emplaced in the basement of epidote-amphibolite- and greenschist-facies metasedimentary rocks [13-14, 18-19 and references therein]. Rehman et al. [20] reported laser ablation inductively coupled plasma mass spectrometry (LA-ICP-MS) U-Pb zircon age of 750 ± 9 Ma for the gray granites and slightly younger ca. 713 ± 32 Ma for the pink granites. Based on identical petrological, mineralogical, geochemical features, similar ages, and occurrence of granitoids in the nearby areas, the NPIC granites were considered as the western extension of the MIS (ca. 745 Ma [21-22]), and correlated with similar granites in the Seychelles islands and those on Madagascar (ca. 750 Ma [23-25]).

Gray granites are composed of perthitic feldspar, plagioclase, quartz, riebeckite-aegirine, and biotite with

accessory zircon, monazite, and apatite [14]. Individual outcrops as well as exposures of pink granites share contacts with gray granites (Fig. 2b). Pink granites are composed of orthoclase phenocrysts armored by sodic plagioclase, displaying the rapakivi texture. Perthite, quartz, plagioclase, biotite, and alkali amphibole form the main mineral assemblage, whereas titanite, rutile, magnetite, apatite, monazite and zircon are the accessories.

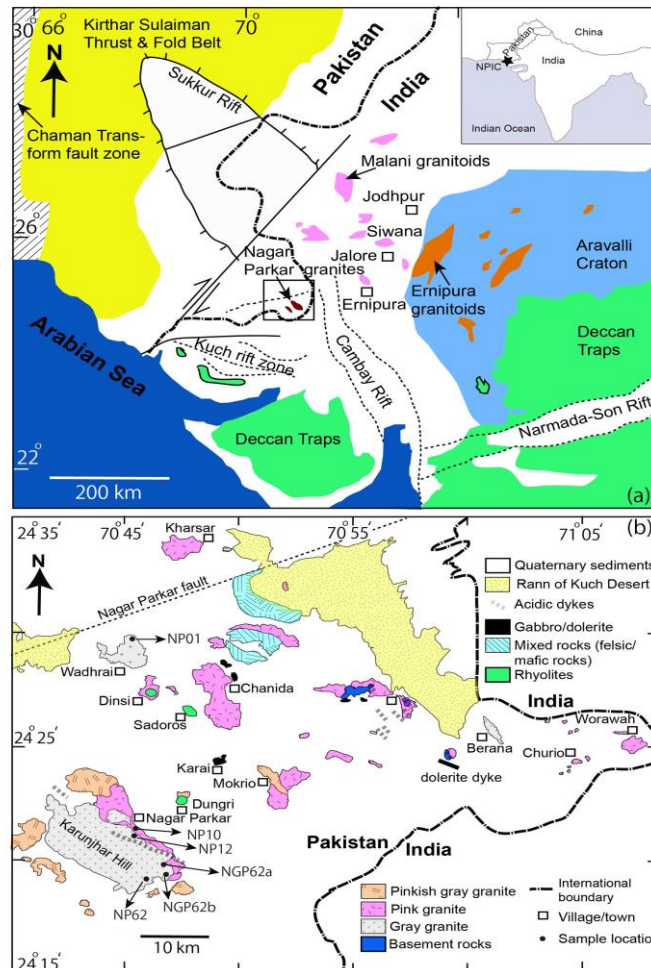


Fig. 2. (a) A simplified geological map of the Nagar Parkar Igneous Complex and Malani Igneous Suite [modified after 12-14, 18-20 and references therein]. The inset at the top right denoted with a filled star indicates the location of NPIC within the Indian-subcontinent. (b) Geological map of the NPIC showing the distribution of gray and pink granites and other lithologies. Samples studied in this study are shown.

3. Methods

Zircons crystals from five samples of gray granites and one sample of pink granites were investigated in this study. The crystals were separated using the conventional methods of heavy liquids and finally hand-picked under the binocular microscope. Zircon grains were mounted in epoxy resin, polished until the central domains were exposed, and imaged under the plane and crossed polarized lights of the optical microscope. Backscattered electron

and cathodoluminescence (CL) images of zircon crystals were also acquired using the scanning electron microscope (SEM) with CL and EDX-detectors. Inclusions, exposed at the surface of the grains, were identified using the SEM-EDX detector, whereas in-depth inclusions were investigated using the RAMAN spectroscopy housed at the Instrumental Analysis Center of the Kagoshima University, Japan. Crystal morphology of the investigated zircons were inspected using the method of Pupin [5], and the data were statistically calculated to obtain the temperature range for the zircon population in each sample. The same grains were analyzed for U–Pb isotope ratios and trace element contents (including Ti) using the LA-ICP-MS. Details of the geochronological results are presented elsewhere [20]. Below, we provide a brief summary of the zircon typology method followed by results.

4. Background of the zircon typology

The zircon typological method, proposed by Pupin [5], is based on the arrangement of prismatic and pyramidal crystal faces that make zircon populations in numerous morphological types, *S-type* as the dominant and most common in nature and other sub-types shown around (Fig. 3). Main types constitute the prisms defined by {100}, {110} with combination of pyramidal faces of either one defined by {101}, {211} or {301}, and the arrangement of {101} and {211}. The main and sub-types were arranged on a square-board that have two variables; the *Indice of alkalinity* “*I.A*” along the horizontal axis, and the *Indice of temperature* “*I.T*” along the vertical axis that depend on the development of prisms and pyramidal crystal faces, respectively. The variable *A* index (*I.A*) represents the development of pyramidal faces with increasing Al/(Na+K) ratios to the right-hand side of the square-board, whereas the variable *T* index (*I.T*) shows the development of prisms with increasing temperature of zircon crystallization downward [5 and earlier studies]. The above two variables were derived as

$$I.A = \sum_{I.A=100}^{800} I.A * n_{I.A} \text{ and } I.T = \sum_{I.T=100}^{800} I.T * n_{I.T}$$

where the $n_{I.A}$ and $n_{I.T}$ represent the respective frequencies of each value of *I.A* or *I.T* in the range from 100 to 800. In addition, zircon populations from the typological approach were plotted on the genetic classification diagram of granitoids that were either derived from crustal or mainly crustal origin (aluminous types), hybrid granites of crust + mantle origin (calcalkaline and subalkaline), and mantle or mainly mantle origin (alkaline and tholeiitic series) as proposed by Pupin [5]. Application of typological approach alone was argued by Vavra [16] because it involves external morphology and derivation of the petrogenetic source is based on the statistical approach. Instead, growth zones (internal structures, best viewed through the cathodoluminescence imaging) combined with the external morphology provide additional information regarding the magmatic crystallization and source determination [6]. The above author interpreted the high and constant growth rates of {010} prisms relative to the symmetric growth of {011} pyramidal faces to have been crystallized in alkaline granitoids. In contrast, relatively fluctuating or gradually decreasing growth rates of {010} prisms and highly variable growth rates of {011} pyramids were attributed to calcalkaline granitoids. Vavra [16] described four controlling factors for the development of the zircon morphology: (1) high cooling rates in alkaline magmas, (2) magma mixing to form calcalkaline series rocks, (3) enrichment of H₂O and trace elements in the residual liquids evolving to calcalkaline

or anatectic magmas, and (4) major element chemistry, particularly the Na+K/Al ratio i.e. the alpaicity. Information obtained from the zircon external and internal morphology provides useful insights in understanding the magmatic crystallization and source petrogenesis. In forthcoming sections, we describe external and internal morphology of the investigated zircons and interpret our observations regarding the crystallization temperatures and their petrogenetic source.

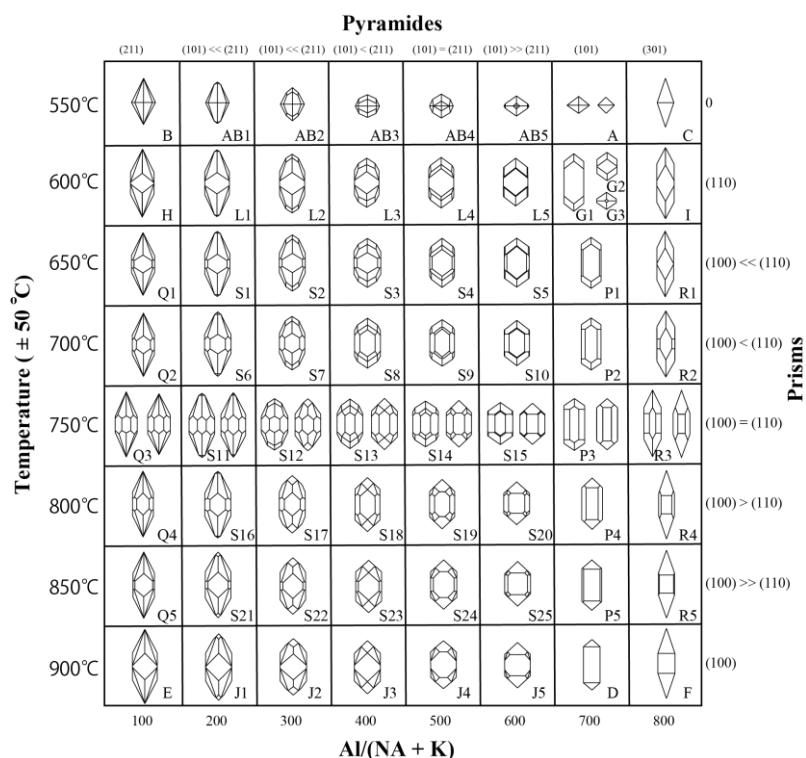


Fig. 3. Zircon crystal typological classification diagram (reproduced from Pupin [5]).

5. Results

Sample used in this study are marked on the geological map (Fig. 2b). Representative zircon grains from the six samples are shown in Figure 4. Internal structures of zircons with growth zones are displayed in Figures 5–10, and the population percent for typological sub-types is given in Figure 11. Estimated temperature values for each sample are summarized in Table 1 and the data plotted in Figure 12. Finally, the zircon typological forms are transposed on the petrogenetic classification diagram of Pupin for source determination (Fig. 13).

5.1. Sample NGP62a (Gray granite)

Twenty-four zircon crystals were investigated from sample NGP62a. Most of the grains were euhedral, colorless to pale pink, and concentrically zoned. The grain size varied from 100–250 μm and contained abundant inclusions of apatite (needle-like network, Fig. 4a), rare monazite, xenotime, and ilmenite. Majority of the grains exhibit

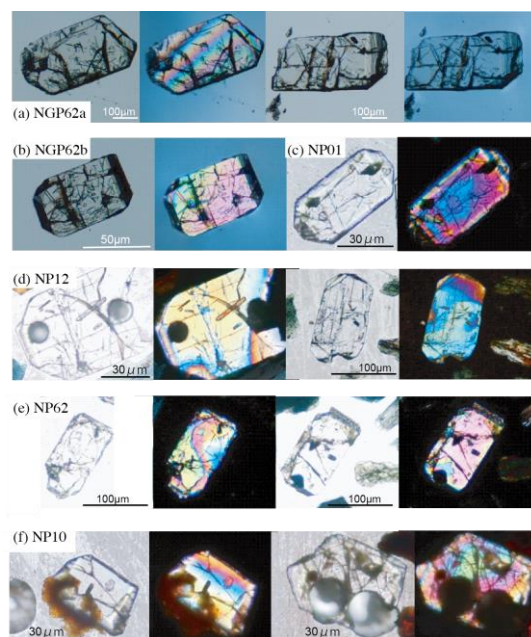


Fig. 4. Photomicrographs (under the optical microscope in plane and crossed polars) showing the crystal shapes of zircons from gray and pink granites. Needle-shape or elongated inclusions are apatite whereas black/opaque phases are ilmenite. Circular pits in some grains are the LA-ICP-MS analysis spots (for the U–Pb and trace elements).

oscillatory zoning with CL-bright cores or central domains and CL-dark rims or outer domains (Fig. 5). The crystals were characterized by predominantly $\{100\}$ or $\{110\}$ prisms and $\{211\}$ and $\{121\}$ pyramidal faces, exhibiting intermediate $I.A$ with low $I.T$ indices for the S_4 – S_5 morphological sub-types and intermediate $I.A$ with relatively high $I.T$ indices for the S_{19} – S_{20} and a few exhibit P_2 – P_5 morphological sub-types (Fig. 3). Some of the zircon crystals were broken but the typological sub-types were inferred from their internal structures (truncations along the pyramidal faces) and presence of the $\{100\}$ or $\{110\}$ prisms, and symmetric growth zoning. Temperature estimates based on crystal shapes show a range of 633–831 $^{\circ}\text{C}$ (n: 24) (Fig. 12a, Table 1). Titanium contents (ppm: as parts per million) in the analyzed zircons range from 2–9 ppm (a few spots with anomalously higher Ti contents were discarded for the possibility of incorporating Ti-bearing inclusion phases). Temperature values, calculated from Ti-in-zircon thermometry after the method of Watson et al. [17], of 631–728 $^{\circ}\text{C}$ (n: 30) were obtained from the analyzed zircons (Table 2). The population of zircons plot in the granodiorites-monzogranites field, with a slight shift towards alkaline granites on the petrogenetic classification diagram (Fig. 13a).

Table 1. Sample details, zircon crystal typology and estimated temperature ranges.

Sample	Rock type	Number of grains	Crystal shape sub-category	T (°C) range based on crystal shape (Average T)	T (°C) range based on Ti-in-zircon (Average T)
NGP62a	Gray granite	24	S ₄ ~S ₅ and S ₁₈ ~S ₂₀	633~831 (742)	631~728 (645)
NGP62b	Gray granite	78	S ₄ and S ₁₈ ~S ₂₀	650~850 (751)	649~841 (725)
NP12	Gray granite	31	S ₁₈ ~S ₂₀	675~810 (796)	634~804 (703)
NP62	Gray granite	56	S ₁₈ ~S ₂₀	613~850 (760)	642~823 (705)
NP01	Gray granite	37	S ₅ and S ₁₈ ~S ₂₀	600~850 (725)	663~796 (736)
NP10	Pink granite	7	S ₉ ~S ₁₀	675~800 (729)	680~782 (725)

5.2. Sample NGP62b (Gray granite)

Seventy-eight zircon grains were investigated from sample NGP62b. Majority of the crystals were euhedral, with abundant inclusions of apatite, plagioclase, monazite, xenotime, and ilmenite (Fig. 4b). Zircon crystals were characterized by predominantly {100} or {110} prisms and {211} and {121} pyramidal faces (Fig. 6). The intermediate *I.A* and low *I.T* indices suggest S₄–S₅, S₉–S₁₀ morphological sub-types, and intermediate *I.A* and relatively high *I.T* indices show S₁₉–S₂₀ and S₂₄–S₂₅ sub-types (Fig. 11). Based on CL images, most of the grains portray oscillatory growth zoning with CL-bright cores and CL-dark outer domains, however a few grains showed the opposite, exhibiting CL-dark centers overgrown by CL-bright domains (Fig. 6). Temperature estimates from the crystal shapes ranged from 650–850°C (n: 78) (Fig. 12b, Table 1). Titanium contents in the analyzed zircons ranged from 2–28 ppm, yielding temperature values of 649–841 °C (n: 36) (Table 2). Zircon population from this sample also plot in the granodiorites-monzogranites fields on the petrogenetic classification diagram (Fig. 13b).

5.3. Sample NP12 (Gray granite)

Thirty-one zircon crystals were characterized by the euhedral shapes with well-developed crystal faces (Figs. 4d & 7). Dominant type of zircons in this sample were {100} type as evidenced from the CL images, however {110} types were also present (Fig. 7). Homogeneous and symmetric growth zoning is exhibited by the CL-bright

centers and CL-dark rims. A few grains showed irregular zoning (grain shown at the lower right corner in Fig. 7). Dominant sub-type of crystals in this sample was S_{20} , with a few grains exhibiting S_{19} , S_9 , and P_4 sub-types (Fig. 11). Temperature values of 675–810°C (n: 31) were obtained from the studied zircons (Fig. 12c, Table 1). Titanium contents ranged from 2–19 ppm that yielded temperature values of 634–804 °C (n: 29) (Table 2). On the petrogenetic classification diagram, the zircons show granodiorites-monzogranites (Fig. 13c).

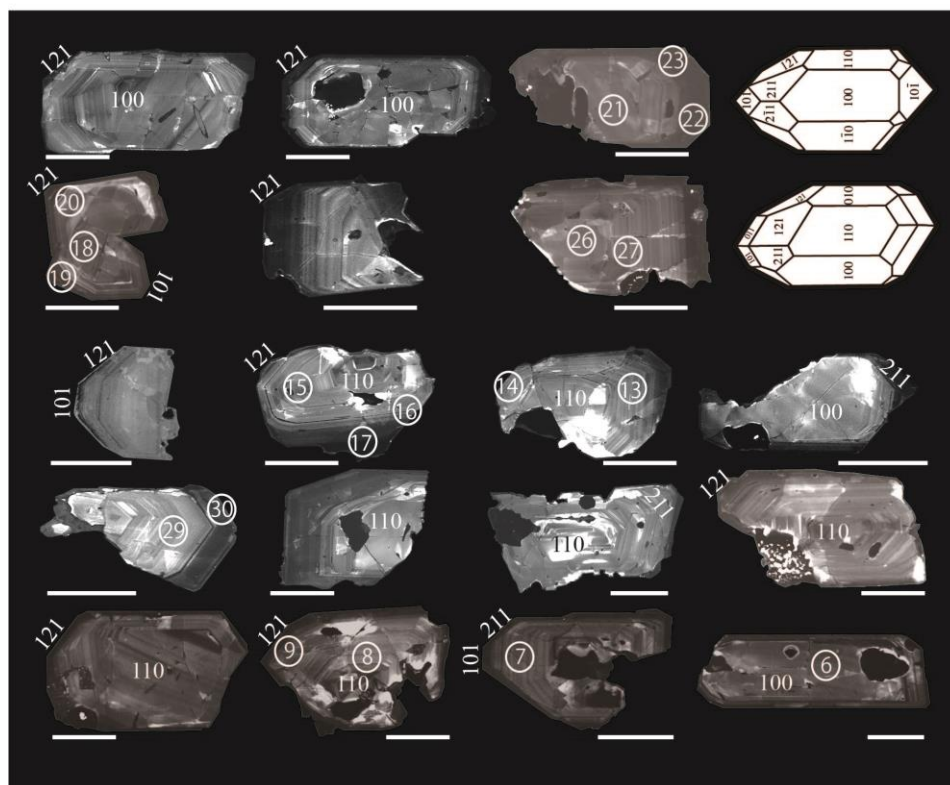


Fig. 5. Cathodoluminescence images of zircons (Sample NGP62a, gray granite) displaying crystal faces and growth zones. For comparison, typical crystal shape of zircon for type {100} and {110} are shown at the top right. Zircon grains (here and in the forthcoming figures) are reoriented to show the long axis in horizontal. Scale bar is 100 μm .

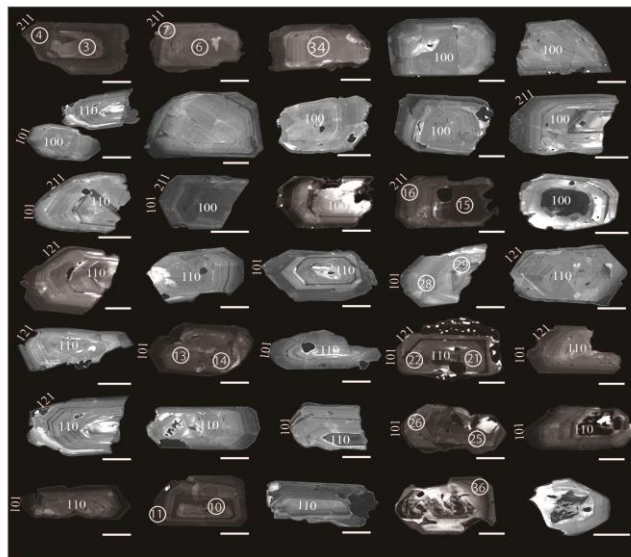


Fig. 6. Cathodoluminescence images of zircons (Sample NGP62b, gray granite) with dominant crystal faces and growth zones. Other features are same as explained in Fig. 5.



Fig. 7. Cathodoluminescence images of zircons (Sample NP12, gray granite) with dominant crystal faces and growth zones. Other features are same as explained in Fig. 5.

5.4. Sample NP62 (Gray granite)

Fifty-six grains from sample NP62 were investigated and the results are shown in Table 1. External forms of representative grains (Fig. 4e) show euhedral grains with well-developed {100} and {110} prisms and {211}, {101}, and {121} pyramidal faces, also identified from the CL images (Fig. 8). Oscillatory zoning and homogeneous growth rates are exhibited by CL-bright centers and CL-dark concentrically grown rims. A few grains display irregular zoning pattern. Majority of zircons show S_{19} – S_{20} sub-types, a few grains of S_9 – S_{10} and P_1 – P_5 sub-types were also identified. Temperature values, based on the crystal shape, range from 613–850°C (n: 56) (Fig. 12d, Table 1) and the temperatures from Ti-in-zircon thermometry showed a range of 659–905 °C (n: 40) (Table 2). Zircons from this sample exhibit relatively large scatter on the petrogenetic classification diagram where the data plot in fields of granodiorites-monzogranites, with several grains plot in the field of alkaline granites (Fig. 13d).

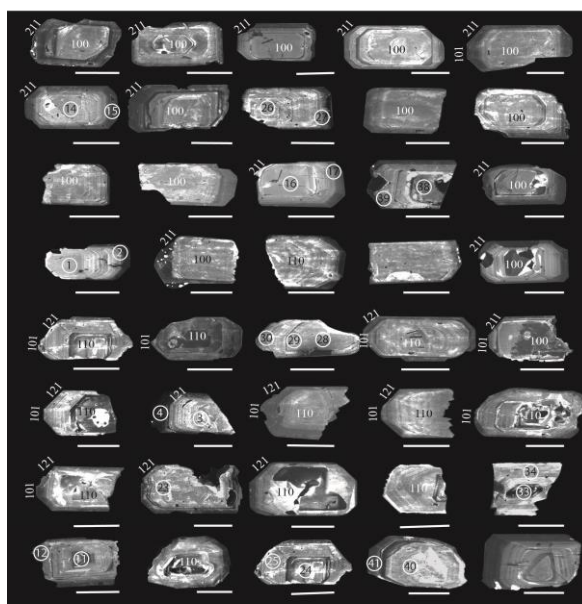


Fig. 8. Cathodoluminescence images of zircons (Sample NP62, gray granite) with dominant crystal faces and growth zones. Other features are same as explained in Fig. 5.

5.5. Sample NP01 (Gray granite)

Thirty-seven zircon crystals were investigated from this sample and results are shown in Table 1. Most of the zircons exhibit euhedral crystals grains with well-developed {100} and {110} prisms and {211}, {101}, and {121} pyramidal faces (Fig. 9). Oscillatory zoning is exhibited by CL-dark centers rimmed by CL-bright rims (in most cases) and CL-bright (a few grains) centers rimmed by CL-dark rims, majority of which display concentric growth zoning with a few exceptions. Dominant sub-types of zircon crystals in this sample were S_{19} – S_{20} and S_4 – S_5 , a few S_9 – S_{10} and S_{14} – S_{15} , and several grains of sub-type P_1 – P_4 (Fig. 11). One grain exhibited S_6 sub-type. Temperature values of 600–850°C (n: 37), based on the crystal shape, were obtained from this sample (Fig. 12e, Table 1) that

are consistent with the Ti-in-zircon thermometry data (range: 663–796 °C, n: 31) (Table 2). Zircon population mark some scatter on the petrogenetic classification diagram but the data plot in granodiorites-monzogranites fields, however a few grains with higher *I.A* index suggest alkaline granites (Fig. 13e).



Fig. 9. Cathodoluminescence images of zircons (Sample NP01, gray granite) with dominant crystal faces and growth zones. Other features are same as explained in Fig. 5.

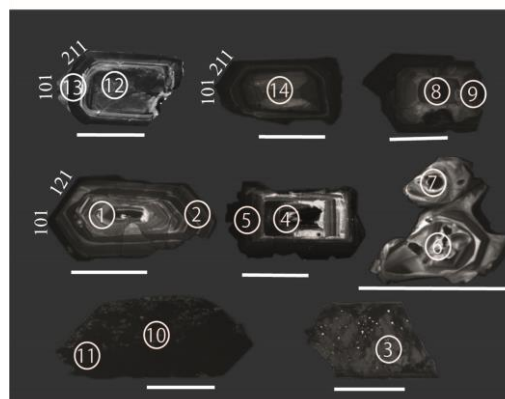


Fig. 10. Cathodoluminescence images of zircons from pink granite (Sample NP10). Other features are same as explained in Fig. 5.

5.6. Sample NP10 (Pink granite)

Only seven zircon crystals were investigated from a sample (NP10) of pink granite (Fig. 4f & 10). The reason for fewer number of grains is because of the smaller size of the sample crushed, and several grains were discarded from statistical calculations for their incomplete crystal shapes and it was impossible to recognize their crystal sub-types. Among the investigated zircons, three crystals exhibited well-developed {100} prims with {211}, {101}, and {121} pyramidal faces, whereas other two grains showed {110} prims with {101} and {121} pyramids (Fig. 10). Two large grains (bottom row of Fig. 10) exhibited skeletal structure with no internal growth zoning but had well-developed prismoid and pyramidal faces. Two other grains (shown in the right middle of Fig. 10) were fused to each other, possibly recrystallized or affected by some late-stage event that is why they yielded discordant and very young U–Pb age values (ca. 154 ± 29 Ma, see Rehman et al. [20]). Zircons from pink granite showed S_9 – S_{10} and S_{19} – S_{20} morphological sub-types (Fig. 11). Temperature values from the crystal shapes range from 675–800 °C (n: 7) (Table 1). Titanium contents range from 4–15 ppm that produced temperatures of 680–782 °C (n: 12) (Table 2). The crystal shape data indicate monzogranites (Fig. 13f).

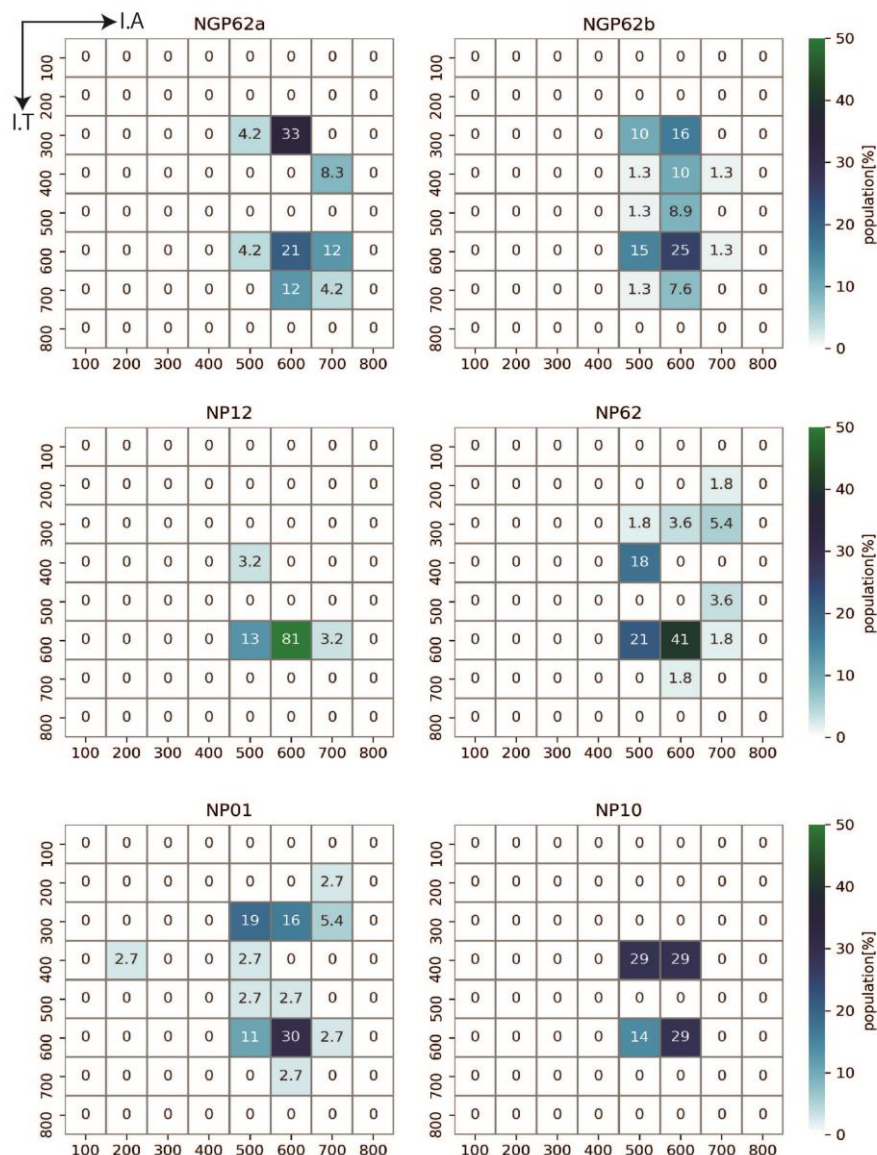


Fig. 11. Plots displaying the populations of zircon sub-types based on typological approach of Pupin. Numbers in square-boxes denote the zircon crystal shape population in percent. Note, majority of zircons from the six granitic samples portray S_4 – S_5 , S_9 – S_{10} , and S_{18} – S_{20} , with a few grains of P_1 – P_4 typological sub-types of zircon.

6. Interpretation of results

6.1. Zircon typology

Zircon typology, combined with internal structures, trace element composition, and U–Pb isotope geochemistry, provides records of magmatic crystallization, petrogenetic source, and thermal history of the rocks that host those

Table 2. Titanium contents (ppm) of the analyzed zircons and the temperature values.

Sample	NGP62a																			
Spot#	#1	#2	#3	#4	#5	#6	#7	#8	#9	#10	#11	#12	#13	#14	#15	#16	#17	#18	#19	#20
Ti (ppm)	2.74	109.37	2.86	2.79	2.58	2.73	2.71	2.54	2.88	2.66	2.57	2.68	2.93	3.10	2.49	3.08	68.43	2.80	5.35	2.98
T (°C)	639	incl	642	640	635	638	638	633	642	637	634	637	643	648	632	647	incl	640	689	645
Spot#	#21	#22	#23	#24	#25	#26	#27	#28	#29	#30										
Ti (ppm)	2.77	3.63	3.59	2.52	2.47	2.67	2.71	2.90	2.75	8.61										
T (°C)	639	639	658	633	631	637	638	643	639	728										
Average T	645																			
Sample	NGP62b																			
Spot#	#1	#2	#3	#4	#5	#6	#7	#8	#9	#10	#11	#12	#13	#14	#15	#16	#17	#18	#19	#20
Ti (ppm)	<2.20	25.69	<2.50	12.91	<2.51	9.97	8.30	4.60	8.91	<2.84	32.70	4.30	<3.30	37.46	<2.99	59.62	<2.95	5.14	<2.72	28.21
T (°C)	-	831	-	764	-	741	725	677	731	-	incl	672	-	incl	-	incl	-	686	-	841
Spot#	#21	#22	#23	#24	#25	#26	#27	#28	#29	#30	#31	#32	#33	#34	#35	#36				
Ti (ppm)	3.15	8.22	26.01	8.22	<3.57	255.35	<2.55	<3.07	4.67	4.47	473.13	<2.57	<2.92	<2.41	<3.39	3.19				
T (°C)	649	724	833	724	-	incl	-	-	678	675	incl	-	-	-	-	650				
Average T	725																			
Sample	NP12																			
Spot#	#1	#2	#3	#4	#5	#6	#7	#8	#9	#10	#11	#12	#13	#14	#15	#16	#17	#18	#19	#20
Ti (ppm)	2.58	5.61	7.32	32.28	47.42	116.04	4.23	6.29	3.19	6.70	3.98	<2.66	14.41	4.96	7.27	5.71	3.51	16.70	45.46	11.41
T (°C)	634	693	714	incl	incl	incl	671	702	650	707	666	-	774	683	714	694	657	788	incl	753
Spot#	#21	#22	#23	#24	#25	#26	#27	#28	#29											
Ti (ppm)	13.35	3.19	19.56	30.84	2.91	5.68	3.53	<2.22	10.36											
T (°C)	767	650	804	incl	643	694	657	-	744											
Average T	703																			
Sample	NP62																			
Spot#	#1	#2	#3	#4	#5	#6	#7	#8	#9	#10	#11	#12	#13	#14	#15	#16	#17	#18	#19	#20
Ti (ppm)	<2.56	3.89	10.72	49.83	5.15	4.32	4.68	<2.98	7.38	4.53	6.19	5.13	4.04	5.32	18.57	<3.50	6.58	3.64	12.34	22.73
T (°C)	-	664	747	905	686	672	678	-	715	676	700	686	667	688	798	-	705	659	760	819
Spot#	#21	#22	#23	#24	#25	#26	#27	#28	#29	#30	#31	#32	#33	#34	#35	#36	#37	#38	#39	#40
Ti (ppm)	56.74	38.00	<3.13	4.40	8.14	10.25	2714	13.60	<2.64	6.75	3.46	23.73	7.24	7.12	3.03	2.87	235.48	<3.37	3.76	4.37
T (°C)	incl	incl	-	674	723	743	incl	769	-	708	656	823	713	712	646	642	incl	-	662	673
Average T	712																			
Sample	NP01																			
Spot#	#1	#2	#3	#4	#5	#6	#7	#8	#9	#10	#11	#12	#13	#14	#15	#16	#17	#18	#19	#20
Ti (ppm)	16.36	15.64	120.82	10.43	36.22	47.93	16.15	35.21	6.30	59.76	16.80	5.81	97.16	109.82	5.59	114.30	9.67	44.86	47.72	5.82
T (°C)	786	782	incl	745	incl	incl	785	incl	702	incl	789	695	incl	incl	692	incl	738	incl	incl	696
Spot#	#21	#22	#23	#24	#25	#26	#27	#28	#29	#30	#31									
Ti (ppm)	262.96	59.16	6.45	145.39	16.11	5.81	148.28	3.84	7.64	18.13	38.59									
T (°C)	incl	incl	704	incl	785	695	incl	663	718	796	incl									
Average T	736																			
Sample	NP10																			
Spot#	#1	#2	#3	#4	#5	#6	#7	#8	#9	#10	#11	#12	#13	#14						
Ti (ppm)	4.87	49.42	93.67	67.95	15.64	33.12	15.13	6.75	77.92	1282	1062	8.03	4.81	29.52						
T (°C)	681	incl	incl	incl	782	incl	779	708	incl	incl	incl	722	680	incl						
Average T	725																			

Foot note to table 2: Temperatures from Ti-in-zircon thermometry are calculated after [17], using the equation: $\log(T_{\text{zircon}}) = [6.01 \pm 0.03] - 5080 \pm 30/T \text{ (K)}$. Titanium contents were determined by LA-ICP-MS analysis (U–Pb age data for the same zircons are reported elsewhere [20]). The term “incl” means the analyses were likely conducted on the Ti-rich inclusion phases (rutile, ilmenite, or titanite). Some of the zircon grains showed Ti contents below the detection limits of the LA-ICP-MS analysis, hence the temperature data are not shown for those spots.

zircon [5, 26-28]. Zircon crystal faces develop progressively with the compositional evolution of granitoid melts [5, 15-16]. However, various morphologies of zircons in a same magma, similar morphological types from different rock types, and periodic changes in the zircon crystal shape representing single growth event [2] pose difficulties to the application of typological method. External and internal crystal morphology of zircon is a strong tool to understand the petrogenetic source and the nature of magma from which the zircons crystallized.

Granites of the NPIC, based on the whole-rock geochemistry, were categorized mainly of crustal origin with minor hybridization of the mantle component, possibly derived from sodic alkaline magma (gray granites) that evolved to per-aluminous [13, 19]. Based on age-data and mineral paragenesis, gray granites are early formed and contain abundant mafic xenoliths. Pink granites were likely derived from the more evolved magma that also likely assimilated the country rocks to some extent. However, secondary processes (possible alteration or sample heterogeneity) may have affected the primary chemical signatures of the whole-rock, therefore interpreting whole-rock bulk chemical compositions may not provide robust information for the granite origin. Past publications (e.g., [18-19]) reported gray and pink granites as within-plate A-type granitoids based on major and trace element geochemistry and particularly the high-field-strength elements ratios (discrimination diagrams [29, 30]). Zircon, a highly resistant to alteration and secondary processes, helps in assessing the geochemical, geochronological, and petrogenetic information of the parent magma.

Pupin [5] interpreted symmetric growth of zircon in water-rich granites that are developed due to deuteric processes associated with secondary minerals (e.g. sericitization, transformation of ferromagnesian minerals and so on). In contrast, mixed morphological forms of zircon commonly grow in granites of mantle and mainly mantle origin (alkaline series) that are derived from hot and dry magmas, characterized by ring-perthites and melanocratic minerals (e.g. aegirine augite, hedenbergite, riebeckite, annite). Presence of some zircon grains with mixed morphologies in the studied samples corroborate the possibility of magma hybridization from different sources. As reported by Belousova et al. [3], morphological variation within single zircon grains indicate magma mixing and progressive crystallization. The relatively smaller variation in zircon morphology in this study suggest the grains likely crystallized in a homogeneous crustal magma that followed a progressive fractional crystallization which facilitated uniform growth domains in zircons. A few irregularly zoned zircons and their asymmetric growth might have formed from a mingled magma during its later stages of crystallization, that possibly incorporated mafic components from the mantle material. These features are consistent with the interpretations reported by earlier researchers for fractional crystallization as evidenced by the perthitic growth of K-feldspar surrounded by plagioclase [14]. Tucker et al. [31] interpreted a juvenile crustal source for granitoids of Seychelles Islands (having ϵNd : +2.85 and higher $\text{Sr}_{\text{initial}}$ ratio: 0.7031) of alkaline to meta-aluminous series. Other granitoids from the nearby areas (e.g., Praslin group also yielded ϵNd : - 1.1 to - 3.8 and $\text{Sr}_{\text{initial}}$ ratios: 0.707 to 0.7163) were likely evolved from the ancient crust [31]. We do not know Sr and Nd isotope compositions of the NPIC granites yet, but similar granites on MIS, Seychelles, and Madagascar, place them in same tectonic entity before the break-up of Rodinia, they might have been derived from a similar source.

6.2. Temperature estimates from the crystal shapes

Temperature data deduced from the zircon crystal morphology, exhibiting a range of 630–850 °C, indicate a plausible temperature range for the granitic magma to crystallize. The temperature values obtained from the zircon crystal shape are consistent with the results obtained from Ti-in-zircon thermometry ($< \pm 50$ °C for four samples and $< \pm 100$ °C for zircons for two samples) (Fig. 12).

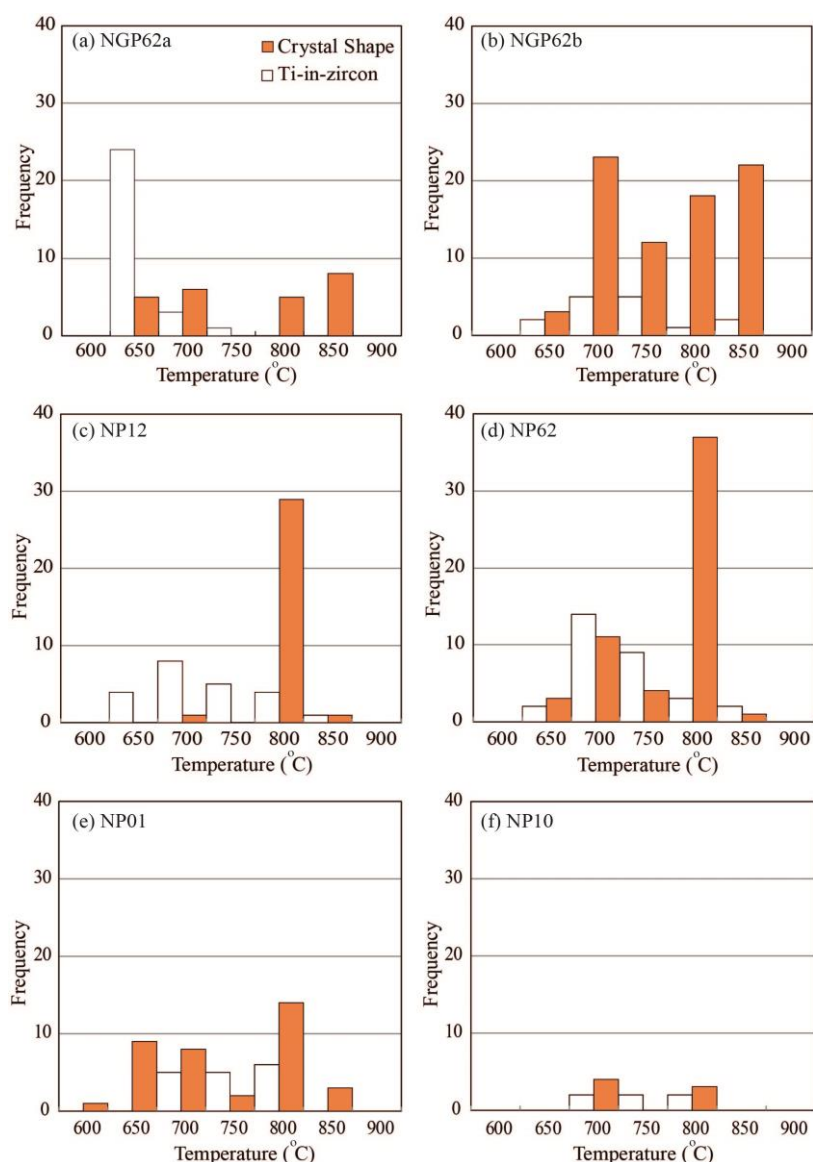


Fig. 12. Histograms displaying temperature values estimated from the external typology of zircon population. Ti-in-zircon thermometry results are also plotted for comparison.

Majority of the zircon crystals, investigated from the six granitic samples, exhibit granodiorite/granitic fields and a few grains shift towards alkaline granites on the petrogenetic classification diagram. These features are consistent with the field and geochemical observations. We assume, our results and interpretations are geologically meaningful and the zircon crystal morphology approach is applicable even for zircons that have been derived from

highly altered rocks or of unknown source. Presence of abundant apatite and some monazite and xenotime in the investigated zircons and their higher relativity with the *I.A* index bear similar conclusion to those described in [5], representing sialic granites of mainly crustal origin with minor hybridization of the mantle.

6.3. *Petrogenetic source*

It is not straight forward to assign petrogenetic source to the granitic bodies, based on the whole-rock geochemistry alone. However, zircon crystal morphology provides significant clue to decipher the petrogenetic source of the host rock. Typological variation of zircons and abundant inclusions of apatite, monazite, and xenotime suggest per-aluminous to alkaline type granite source that could have been mainly derived from a crustal origin. Whereas, mafic xenoliths and higher *I.A* in some zircons indicate some hybridization of crust with mantle component. Tectonic scenario of the Indian Shield, a part of which is represented by the NPIC granites, involved a subduction margin environment that followed superplume activity in the Rodinia-break up during Neoproterozoic (ca. 750 Ma till 640 Ma; see Rehman et al. [20] for details). Homogenous growth zoning of zircons, characterized by well-developed {100} and {110} prisms, and {101}, {211}, and {121} pyramids indicate their formation/growth in per-aluminous magma that slightly evolved to alkaline type.

Crustal cooling combined with magmatic differentiation and assimilation can also be read from the zircon crystal shapes. Relative variation in zircon crystal morphology and temperature range of 630–850 °C, could be attributed to the crystallization process of magma. Mixed morphological zircons suggest relatively evolved magma during which the temperature of crystallization proceeded from higher (> 850°C) to relatively lower values (< 650 °C). Our results are consistent with the interpretations of recently reported U–Pb zircon age data for the NPIC granites. The age spectrum (ca. 773–640 Ma) suggests continuous crustal growth and possible fractional crystallization of magma that was recorded in the concentrically zoned zircons [20]. Ti-in-zircon thermometry (631–840 °C, Table 2) is consistent with temperature data obtained from the zircon morphology. Moreover, morphology of the investigated zircons indicates monzogranites as their petrogenetic source with a slight shift towards alkaline granites (Fig. 13). These results are consistent with the information available from the field geology. Based on these pieces of evidence, we conclude that crystallization of zircon, in magma that formed gray and pink granites, initiated around 900–850 °C and cooled until 650 °C. Zircon crystal morphology is a strong tool that provides information regarding the temperatures of the magmatic crystallization and their petrogenetic source.

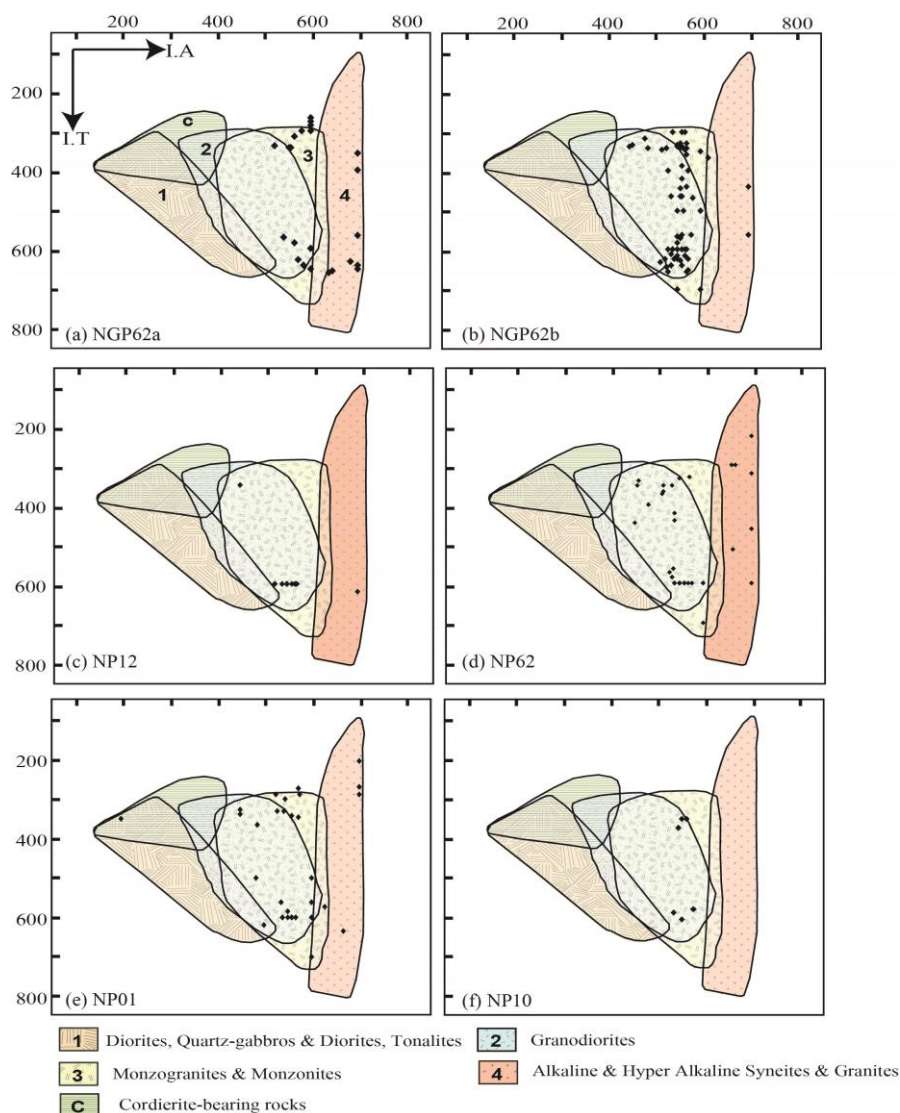


Fig. 13. Petrogenetic classification diagram based on zircon crystal typology. Most of the zircons from gray and pink granites plot in the monzogranite/granodiorite fields and a few grains show alkaline granites (adopted from [5]).

Acknowledgements

We thank Kubo, S and Ohkura, R (Kagoshima University Institute of the Instrumental analysis) for their support during the analysis. Due thanks to Lee, H.Y. Emily H, and Terry, T of Academia Sinica, Taiwan, for their help during the CL images and Ti-in-Zircon analysis. Yamamoto, H. of Kagoshima University is thanked for useful discussions and advice. Our sincere thanks to Khan, T. for providing the granite samples for this study. This work was partly supported by special fund for Science Club activities from the Dean, Faculty of Science, Kagoshima University, and partly by the JSPS research fund (Kakenhi # 15K05316 to HUR).

References

- [1] P.W.O. Hoskin, T.R. Ireland, *Geology* 28 (2000), 627-630.
- [2] P.W.O. Hoskin, U. Schaltegger, *Rev. Min. Geochem.* 53 (2003), 27-62.
- [3] E.A. Belousova, W.L. Griffin, S. Y. O'Reilly, 2006. *Jour. Pet.* 47 (2006), 329-353.
- [4] E.E. Scherer, M.J. Whitehouse, C. Münker, *Elements* 3 (2007), 19-24.
- [5] J.P. Pupin, *Cont. Min. Pet.* 73 (1980), 207-220.
- [6] G. Vavra, *Cont. Min. Pet.* 106 (1990) 90-99.
- [7] F. Corfu, J.M. Hanchar, P.W.O. Hoskin, P. Kinny, *Rev. Min. Geochem.* 53 (2003), 468-500.
- [8] D. Rubatto, D. Gebauer, *Cathodoluminescence in Geosciences* (2000) 373-400.
- [9] H.C.B. Martins, P.P. Simões, J. Abreu, *Compt. Rend. Géos.* 346 (2014), 233-243.
- [10] R.J.M. Taylor, C.L. Kirkland, C. Clark, *Lithos* 264 (2016), 239-257.
- [11] M. Hayashi, *Jour. Geol. Soc. Jap.* 96(1990), 117-123.
- [12] A.H. Kazmi, R.A. Khan, *Geol. Surv. Pak. Info. Rel.* 64 (1973), 1-32.
- [13] M.Q. Jan, A. Laghari, M.A. Khan, *Geol. Bul. Uni. Pesh.* 30 (1997), 227-249.
- [14] T. Khan M. Murata, H.U. Rehman, M. Zafar, H. Ozawa, *Jour. Asia. Ear. Sci.* 59 (2012), 39-51.
- [15] G. Vavra, *Chem. Geol* 110 (1993), 15-28.
- [16] G. Vavra, *G. Cont. Min. Pet.* 117 (1994), 331-344.
- [17] E.B. Watson, D.A. Wark, J.B. Thomas, *Cont. Min. Pet.* 151 (2006), 413-433.
- [18] M.Q. Jan, M.H. Agheem, A. Laghari, S. Anjum, 2017. *Jour. Geol. Soc. India* 89 (2017), 91-98.
- [19] T. Khan, M. Murata, M.Q. Jan, H.U. Rehman, M. Zafar, H. Ozawa, A. Qadir, S. Mehmood, *Arab. Jour. Geosci.* 10:308 (2017), DOI: 10.1007/s12517-017-3077-y.
- [20] H.U. Rehman, T. Khan, M.Q. Jan, H-Y. Lee, S-L. Chung, M. Murata, *Gond. Res.* 61 (2018), 172-186.
- [21] A.R. Crawford, W. Compston, *Quart. Jour. Geol. Soc. London* 125 (1969), 351-371.
- [22] J.G. Meert, M.K. Pandit, G.D. Kamenov, *Tectonophysics* 608 (2013), 1254-1267.
- [23] M. Hoshino, *Lithos* 19 (1986), 11-25.
- [24] T.H. Torsvik, L.D. Ashwal, R.D. Tucker, E.A. Eide, *Precambrian Research* 110 (2001), 47-59.
- [25] L.D. Ashwal, A.M. Solanki, M.K. Pandit, F. Corfu, B.W.H. Hendriks, K. Burke, T.H. Torsvik, *Prec. Res.* 236 (2013), 265-286.
- [26] B. Barbarin, *Rend. Del. Soc. Ita. di min.e Pet.* 43-2(1988), 463-476.
- [27] Y. Noumi, K. Wadatsumi, S. Matsumoto, 1997. *Geoinfor.* 8 (1997), 149-156.
- [28] S. Ikeda, Y. Noumi, *Naturalisae* 21 (2017), 59-68.
- [29] J.B. Whalen, K.L. Curry, B.W. Chappell, *Cont. Min. Pet.* 95 (1987), 407-419.
- [30] W.A. Eby, *Geology* 20 (1992), 641-644.
- [31] R.D. Tucker, L.D. Ashwal, T.H. Torsvik, *Ear. Plan. Sci. Lett.* 187 (2001), 27-38.